Neurochemistry International 126 (2019) 139–153

Contents lists available at ScienceDirect

Neurochemistry International

journal homepage: www.elsevier.com/locate/neuint

Oligodendrocyte degeneration and concomitant microglia activation directs peripheral immune cells into the forebrain

Uta Chrzanowski[a], Sudip Bhattarai[a], Miriam Scheld[b], Tim Clarner[b], Petra Fallier-Becker[c], Cordian Beyer[b], Sven Olaf Rohr[a], Christoph Schmitz[a], Tanja Hochstrasser[a], Felix Schweiger[a], Sandra Amor[d,e], Anja Horn-Bochtler[f], Bernd Denecke[g], Stella Nyamoya[a], Markus Kipp[h,*]

[a] Department of Anatomy II, Ludwig-Maximilians-University of Munich, 80336, Munich, Germany
[b] Institute of Neuroanatomy and JARA-BRAIN, Faculty of Medicine, RWTH Aachen University, 52074, Aachen, Germany
[c] Institute of Pathology and Neuropathology, University of Tuebingen, 72076, Tuebingen, Germany
[d] Department of Pathology, VU University Medical Centre, Amsterdam, the Netherlands
[e] Centre for Neuroscience and Trauma, The Blizard Institute Barts and The London, School of Medicine and Dentistry, Queen Mary University of London, London, UK
[f] Department of Anatomy I, Ludwig-Maximilians-University of Munich, 80336, Munich, Germany
[g] Interdisciplinary Center for Clinical Research, University Hospital RWTH Aachen, Aachen, Germany
[h] Institute of Anatomy, Medical University of Rostock, Rostock, Germany

ARTICLE INFO

Keywords:
Moesin
Multiple sclerosis
Cuprizone
Experimental autoimmune encephalomyelitis

ABSTRACT

Brain-intrinsic degenerative cascades are a proposed factor driving inflammatory lesion formation in multiple sclerosis (MS) patients. We recently showed that encephalitogenic lymphocytes are recruited to the sites of active demyelination induced by cuprizone. Here, we investigated whether cuprizone-induced oligodendrocyte and myelin pathology is sufficient to trigger peripheral immune cell recruitment into the forebrain. We show that early cuprizone-induced white matter lesions display a striking similarity to early MS lesions, i.e., oligodendrocyte degeneration, microglia activation and absence of severe lymphocyte infiltration. Such early cuprizone lesions are sufficient to trigger peripheral immune cell recruitment secondary to subsequent EAE (experimental autoimmune encephalomyelitis) induction. The lesions are characterized by discontinuation of the perivascular glia limitans, focal axonal damage, and perivascular astrocyte pathology. Time course studies showed that the severity of cuprizone-induced lesions positively correlates with the extent of peripheral immune cell recruitment. Furthermore, results of genome-wide array analyses suggest that moesin is integral for early microglia activation in cuprizone and MS lesions. This study underpins the significance of brain-intrinsic degenerative cascades for immune cell recruitment and, in consequence, MS lesion formation.

1. Introduction

Multiple sclerosis (MS) is a neuroinflammatory disorder of the central nervous system (CNS), potentially leading to severe motor, sensory, or visual deficits. Clinically, MS represents one of the main causes of disability in the young adult, and thus has a high socio-economic impact. At the histopathological level, MS lesions are characterized by oligodendrocyte death, demyelination, gliosis, axonal damage, and peripheral immune cell infiltration (Bauer et al., 2001; Benn et al., 2001). Despite decades of research, it is still not clear what causes the formation of new inflammatory lesions in MS patients.

MS can be, based on the disease course, clinically categorized into three groups: relapsing-remitting, secondary progressive, and primary progressive. In most patients, the initial course of the disease is relapsing-remitting which is characterized by acute clinical attacks that are followed by complete or incomplete recovery, and a period of remission in between the attacks. Many patients with an initial relapsing-remitting disease course develop secondary progressive MS. In these patients, a more or less continuous decline of neurological functioning occurs with or without occasional attacks (Lublin et al., 2014). Primary progressive MS is characterized by the accumulation of clinical disability from the onset of symptoms, without early relapses or remissions.

It is broadly accepted that the histopathological correlate of acute attacks is a focal inflammatory demyelinating white matter lesion. These focal inflammatory lesions impact on neuronal integrity eventually leading to axonal dysfunction or complete axonal destruction

* Corresponding author. Institut für Anatomie, Universitätsmedizin Rostock, Gertrudenstraße 9, 18057, Rostock, Germany.
E-mail address: markus.kipp@med.uni-rostock.de (M. Kipp).

https://doi.org/10.1016/j.neuint.2019.03.005
Received 31 July 2018; Received in revised form 21 January 2019; Accepted 6 March 2019
Available online 10 March 2019
0197-0186/

(Ferguson et al., 1997; Kornek et al., 2000). Although the accumulation of peripheral immune cells is a characteristic of such lesions, it is not clear what triggers the influx of immune cells into the central nervous system (CNS). However, a degenerative process within the brain has been suggested as one potential trigger mechanism (De Groot et al., 2001; Barnett and Prineas, 2004; Scheld et al., 2016; Ruther et al., 2017). Indeed, that damage to the brain parenchyma can trigger the site of inflammatory lesion formation, is well known. In both - active immunization and passive transfer forms of experimental autoimmune encephalomyelitis (EAE) - an autoimmune animal model of MS, inflammatory lesions rapidly localize at sites of non-specific brain damage, including thermal brain injury (Levine and Hoenig 1968, 1971), cyanide-induced encephalopathy (Levine, 1960), cortical cryolesions (Phillips et al., 1995; Lake et al., 1999), experimental induction of Wallerian degeneration (Konno et al., 1990), or cytokine injection (Sun et al., 2004). In humans, it has been suggested that mechanical stresses can determine the site of spinal cord MS lesions (Oppenheimer, 1978). These studies clearly illustrate the significance of brain-intrinsic degenerative cascades for immune cell recruitment and MS lesion formation.

We recently demonstrated that cuprizone-induced demyelination can trigger peripheral immune cell recruitment into the forebrain after MOG_{35-55} immunization (Scheld et al., 2016; Ruther et al., 2017). In these studies, demyelination of the murine forebrains was induced by a 3-weeks cuprizone (Cup) intoxication protocol, followed by two weeks on normal chow. At week five, encephalitogenic T cells in peripheral lymphoid organs were generated by active immunization with the myelin oligodendrocyte glycoprotein 35–55 peptide ($MOG_{35–55}$) (Iglesias et al., 2001). While peripheral immune cell recruitment was minimal in the forebrains of $MOG_{35–55}$-immunized mice (i.e., active EAE induction), cuprizone-induced demyelination revealed to be a potent trigger for the recruitment of monocytes, lymphocytes and granulocytes (Scheld et al., 2016; Ruther et al., 2017). A drawback of these previous studies using this so-called Cup/EAE model is, however, that active $MOG_{35–55}$ immunization was induced at a time when demyelination was already fully established. This is in contrast to proposed mechanisms operant during early MS lesion formation, i.e., oligodendrocyte degeneration and microglial activation associated with few lymphocytes and phagocytes in regions of relative myelin preservation (van der Valk and De Groot, 2000; De Groot et al., 2001; Barnett and Prineas, 2004; Marik et al., 2007).

The purpose of this study was, therefore, to investigate whether a short-term cuprizone intoxication protocol is sufficient to trigger peripheral immune cell recruitment after MOG_{35-55} immunization. Additionally, by using gene array technology, we aimed at identifying factors orchestrating immune cell recruitment into the forebrains of Cup/EAE mice. We can show that cuprizone-induced oligodendrocyte degeneration with concomitant microglia activation is sufficient to trigger the recruitment of peripheral immune cells into the forebrain. Of note, the extent of cuprizone-induced tissue injury positively correlates with the number of focal inflammatory lesions after MOG_{35-55} immunization. Results of gene array analyses and immunohistochemical stains suggest an important role of moesin$^+$ microglia for the formation of the inflammatory foci.

2. Materials and methods

2.1. Animals and experimental groups

8 week-old C57BL/6 female mice (19 g - 20 g) were purchased from Janvier Labs (Le Genest-Saint-Isle, France). Microbiological monitoring was performed according to the Federation of European Laboratory Animal Science Associations recommendations. A maximum of five animals were housed per cage (cage area 435 cm^2). Animals were kept under standard laboratory conditions (13 h light/11 h dark cycle, controlled temperature 22 °C ± 2 °C and 50% ± 10% humidity) with access to food and water *ad libitum*. It was assured that researchers and technicians did not use any light during the night cycle period. Nestlets were used for environmental enrichment. All experiments were formally approved by the Regierung Oberbayern (reference number 55.2-154-2532-73-15). Mice were randomly assigned to the following groups (see Fig. 3A): (A) control, animals received a diet of standard rodent chow for the duration of the study; (B) 1wk cuprizone (Cup)/EAE, animals were fed a diet containing 0.25% cuprizone (bis(cyclohexanone)oxaldihydrazone; Sigma-Aldrich, Taufkirchen, Germany) mixed into ground standard rodent chow for one week, followed by normal chow for 24 h, and were then immunized with $MOG_{35–55}$ (Hooke Laboratories, Inc., Lawrence, USA) at the beginning of week two; (C) 3wks cup/EAE, animals were fed the cuprizone diet for three weeks, and were then immunized with $MOG_{35–55}$ at the beginning of week four; (D) 3 cup + 2wks normal chow/EAE, mice were fed the cuprizone diet for the first three weeks and were then immunized with $MOG_{35–55}$ at the beginning of week six. Additional animals were fed the cuprizone diet for either 1wk, 3wks, or 5wks and 3 wks + 2wks normal chow without any additional MOG_{35-55} immunization (not shown in Fig. 3A). This experimental setup was published previously (Scheld et al., 2016; Ruther et al., 2017).

2.2. Multiple sclerosis tissues

Paraffin-embedded postmortem brain tissues were obtained through a rapid autopsy protocol from subjects with mainly progressive MS (in collaboration with the Netherlands Brain Bank, Amsterdam). The study was approved by the institutional ethics review board, and all donors or their relatives provided written consent for the use of brain tissues and clinical information for research purposes. Staging of lesions was performed as reported previously (van der Valk and De Groot, 2000; Grosse-Veldmann et al., 2016; Trepanier et al., 2018). In brief, active lesions are defined as hypercellular throughout the entire lesion, chronic active lesions are defined as a lesion with a hypocellular center and a hypercellular rim, and chronic inactive lesions are defined as hypocellular throughout the entire lesion. For the study, three chronic active and three chronic inactive lesions were included. The average age of patients in years was 56.8 ± 14.36 (mean ± SD). The average postmortem delay in hours was 10.02 ± 0.3365. Staging of the white matter lesion activity was performed using anti-PLP and anti-MHC class II (LN3)-stained sections.

2.3. EAE and disease scoring

To induce the formation of encephalitogenic T cells in peripheral lymphatic tissues, mice were subcutaneously immunized with an emulsion of $MOG_{35–55}$ peptide dissolved in complete Freund's adjuvant followed by intraperitoneal injections of pertussis toxin in PBS (PTX) on the day of and the day after immunization (Hooke Laboratories, Inc., Lawrence, USA) as published previously (Ruther et al., 2017). Disease severity was scored as follows: 1, the entire tail drops over the observer's finger when the mouse is picked up by base of the tail; 2, the legs are not spread apart but held close together when the mouse is picked up by base of the tail, and mice exhibit a clearly apparent wobbly gait; 3, the tail is limp and mice show complete paralysis of hind legs (a score of 3.5 is given if the mouse is unable to raise itself when placed on its side); 4, the tail is limp and mice show complete hind leg and partial front leg paralysis, and the mouse is minimally moving around the cage but appears alert and feeding (a score of 4 was not attained by any of the mice in our study).

2.4. Tissue preparation

For histological and immunohistochemical studies, mice were anaesthetized with ketamine (100 mg kg^{-1} i.p.) and xylazine (10 mg kg^{-1} i.p.), and transcardially perfused with ice-cold PBS followed by a 3.7%

formaldehyde solution (pH 7.4). Brains were postfixed overnight in a 3.7% formaldehyde solution, dissected, embedded in paraffin, and then coronal sections (5 µm) were prepared (Acs et al., 2009; Clarner et al., 2012). Spinal cords were incubated in a Na/EDTA (ethylenediaminetetraacetic acid) solution for 48 h (changed once after ~24 h) at 37 °C prior to paraffin embedding. For gene expression studies, tissues were manually dissected after transcardial PBS perfusion, immediately frozen in liquid nitrogen, and kept at −80 °C until further processing.

2.5. Immunohistochemistry/Histochemistry and Evaluation

For immunohistochemistry, sections were rehydrated and, if necessary, antigens were unmasked by heating in Tris/EDTA (pH 9.0) or citrate (pH 6.0) buffer. After washing in PBS, sections were blocked in blocking solution (serum of the species in which the secondary antibody was produced) for 1 h. Then, sections were incubated overnight (4 °C) with primary antibodies diluted in blocking solution. The next day, slides were incubated in 0.3% hydrogen peroxide/PBS for 1 h and then incubated with biotinylated secondary antibodies for 1 h followed by peroxidase-coupled avidin-biotin complex (ABC kit; Vector Laboratories, Peterborough, UK). Sections were finally exposed to 3,3′-diaminobenzidine (DAKO, Santa Clara, CA, USA) as a peroxidase substrate as published previously (Hoflich et al., 2016). To visualize cell nuclei, sections were stained with hematoxylin solution. Negative control sections without primary antibodies or with isotype antibodies were processed to ensure specificity of the staining. Antibodies used in this study are listed in supplementary table 1. Luxol fast blue (LFB)/periodic acid-Schiff (PAS) stains were performed following standard protocols.

Stained and processed sections were digitalized using a Nikon ECLIPSE 50i microscope (Nikon, Nikon Instruments, Düsseldorf, Germany) equipped with a DS-2Mv camera. The open source program ImageJ (NIH, Bethesda, MD, USA) was used to determine staining intensities, cellular densities and to quantify the densities of APP^+ spheroids at specified distances from inflamed vessels (0–100 µm). To evaluate staining intensity using semi-automated densitometrical evaluation after threshold-setting, acquired images were converted to grey scale images, and a global thresholding algorithm was used for dividing each image into two classes of pixels (black and white; i.e., binary conversion). Global thresholding works by choosing a value cutoff, such that every pixel less than that value is considered one class, while every pixel greater than that value is considered the other class. Relative staining intensity was then quantified in binary converted images, and results are presented as percentage area. To quantify the numbers and localization of perivascular cuffs (PVCs) per section in the forebrain, lesions were identified in hematoxylin and eosin (H&E)-stained sections by one evaluator blinded to the treatment groups, and the results were averaged per brain section. Forebrains were analyzed between the levels R215 and R295 according to the mouse brain atlas by Sidman et al. (http://www.hms.harvard.edu/research/brain/atlas.html) as published previously (Ruther et al., 2017). For the analysis of $IBA1^+$ and $CD3^+$ cell densities in mice brains, and $moesin^+$ cell densities in human MS lesions, stained sections were scanned with the Zeiss Mirax Midi scanner (Zeiss, Carl Zeiss MicroImaging GmbH, Jena, Germany) equipped with a Stingray camera, and analyzed with the open source program ViewPoint Online (PreciPoint, Freising, Germany).

2.6. Immunofluorescence labeling

For immunofluorescence labelling, sections were deparaffinized, rehydrated, unmasked, and blocked in serum of the species in which the secondary antibody was raised. Sections were incubated overnight (4 °C) with the indicated combination of primary antibodies diluted in blocking solution. For double-labelling experiments, anti-moesin antibodies were either combined with goat anti-IBA1 for the detection of murine microglia, or anti-MHC-II (LN3) for the detection of activated microglia and monocytes in human tissues. Acute axonal injury was visualized with anti-amyloid precursor protein (APP) antibodies. After extensive washing, sections were incubated with a combination of fluorescent secondary antibodies. Sections were then incubated with Hoechst 33258 (bisBenzimide H 33258 Sigma Aldrich, Steinheim, Germany; 1:10,000) diluted in PBS for the staining of cell nuclei. To exclude unspecific binding of the fluorescent secondary antibodies to primary antibodies, negative controls were performed by first incubating sections with the primary antibodies and subsequently incubating these sections with the "wrong" secondary antibodies. Unspecific secondary antibody binding was excluded by incubating sections with the fluorescent secondary antibodies alone. Stained and processed sections were documented using an Olympus BX51-Wi fluorescence microscope station (Olympus, Germany).

2.7. Transmission electron microscopy

For ultrastructural studies, tissue samples were fixed in 2.5% glutaraldehyde (Science Services, Munich, Germany) cacodylate buffer (pH 7.4; Merck-Millipore, Darmstadt, Germany) at 4 °C overnight as described previously (Noell et al., 2012). Thereafter, samples were embedded in Araldite (Serva, Heidelberg, Germany), and ultrathin sections were cut using a Leica ultramicrotome (Leica, Wetzlar, Germany) and analyzed using a Zeiss EM-10 transmission electron microscope (Zeiss, Oberkochen, Germany).

2.8. Gene array analyses

Genome-wide gene expression of corpus callosum (CC) from control mice and mice fed with cuprizone (male) for 1 week was analyzed in independent quadruplicates using Affymetrix GeneChip® MouseGene1.0 ST Arrays. Total RNA was isolated using RNeasy Kits from QIAGEN, and quantity was assessed using the NanoDrop-1000 Spectrophotometer (Thermo Fisher Scientific, Wilmington, DE, U.S.A.) and RNA quality was assessed using the RNA 6000 NanoChips with the Agilent 2100 Bioanalyzer (Agilent, Waldbronn, Germany). Total RNA samples, each 150 ng, were prepared for the GeneChip® Mouse Gene 1.0 ST Arrays (Affymetrix, USA), and hybridized to the arrays according to the Ambion whole transcript expression and the Affymetrix whole transcript terminal labelling and control kits manuals. Processed samples were hybridized to the GeneChip® Mouse Gene 1.0 ST Arrays at 45 °C for 16 h with 60 rpms, washed and stained on a Fluidics Station 450 (program FS450_00007) and scanned on GeneChip® Scanner 3000 7G (both Affymetrix). Raw image data were analyzed with Affymetrix® Expressin ConsoleTM Software, gene expression intensities were normalized and summarized with robust multiarray average algorithm (Irizarry et al., 2003). To identify genes differentially expressed between cuprizone treated and control mice a comparison analysis using Affymetrix Transcriptome Analysis Console (TAC) 4.0 Software was performed. Gene expression was considered as changed if transcript levels between cuprizone treated and control groups were differential with a 1.5-fold change and a FDR p value of < 0.05. Gene ontology enrichment analysis was performed using the "*Enrichment analysis*" tool (http://www.geneontology.org). The following items were applied: 'GO biological process' for annotation data set, 'Fischer's exact" for test-type, and Bonferroni correction for multiple testing. A list of up- and down regulated genes is provided in supplementary table 2. The microarray data have additionally been deposited in the Gene Expression Omnibus database #GSE119672.

2.9. Statistical analyses

Statistical analyses were performed using Prism 5 (GraphPad Software Inc., San Diego, CA, USA). All data are given as arithmetic means ± SEMs. A p value of < 0.05 was considered to be statistically significant. Applied statistical tests are given in the respective figure

legends. No outliers were excluded from the analyses. No sample size calculation was performed.

3. Results

Histopathological characteristics of initial demyelinating MS lesions are (i) stressed oligodendrocytes with apoptotic-like nuclear changes, (ii) activated microglia, dispersed between seemingly intact myelin, and (iii) few if any lymphocytes (Barnett and Prineas, 2004; Marik et al., 2007; Haider et al., 2011; Prineas and Parratt, 2012). In a first step, we investigated histopathological characteristics of early cuprizone lesions. Numerous apoptotic oligodendrocytes (i.e., condensed and/or fragmented nuclei of cells in a chain-like formation in H&E-stained sections, see arrows in Fig. 1A) were observed in the CC of animals treated with cuprizone for one week. Apoptotic cells were absent in control animals. In both the cortex and the CC, numerous ATF3$^+$ cells were observed in cuprizone-intoxicated but not control animals (Fig. 1B), showing activation of a stress response in oligodendrocytes (Goldberg et al., 2013). Immunohistochemical stains for three distinct myelin proteins, namely proteolipid protein (PLP), myelin-associated glycoprotein (MAG), and 2′,3′-cyclic nucleotide 3′ phosphodiesterase (CNPase), as well as the histochemical stain Luxol Fast Blue/Periodic acid-Schiff (LFB/PAS) demonstrated the absence of demyelination at week 1 (Fig. 1C–F), but severe demyelination after a 5 weeks continuous cuprizone intoxication period. The presence of intact myelin was also evident on the ultrastructural level (Fig. 1J) and verified in anti-myelin protein stained sections by unbiased densitometrical analyses (Fig. 1K). While anti-myelin staining intensities were unchanged after 1 and 3 weeks continuous cuprizone-intoxication, severe anti-PLP, anti-MAG and anti-CNPase staining intensities were observed after 5 weeks continuous cuprizone-intoxication. Anti-ionized calcium-binding molecule 1 (IBA1) staining of control brain sections showed cells with a small cell body and thin, highly ramified cell processes, both characteristics of resting microglia. After 1 week cuprizone exposure, cell processes were swollen and less ramified whereas cell bodies showed hypertrophy, indicating an activated microglia phenotype (Fig. 1G). Furthermore, densities of anti-IBA1$^+$ cells were significantly higher after 1 week of cuprizone intoxication (control: 83.7 ± 11.4 versus 319.6 ± 52.6 cells/mm^2, $p \leq 0.05$). CD3$^+$ and CD4$^+$ lymphocytes were virtually absent in control (0.0 ± 0.0 CD3$^+$ cells/mm^2; n = 5) and 1 week (3.7 ± 1.5 CD3$^+$ cells/mm^2; n = 5) cuprizone-intoxicated animals (Fig. 1H/I). In summary, the histopathological characteristics of the initial demyelinating lesions in MS are well reproduced in mice following a one week cuprizone intoxication protocol.

Next, we investigated whether the observed histopathological changes are sufficient to trigger peripheral immune cell recruitment into the forebrain after MOG_{35-55} immunization. To this end, a second cohort of animals was intoxicated with cuprizone for one week and subsequently immunized with MOG_{35-55} peptide (group B in Fig. 3A). A previous study reported that cuprizone intoxication in mice halts T cell mediated autoimmunity (Mana et al., 2009). We, thus investigated whether the severity of clinical symptoms in classical MOG_{35-55}-immunized EAE mice was comparable in animals with or without previous cuprizone intoxication. Consequently, clinical scores were daily recorded and compared to mice fed normal chow prior to active EAE induction. No significant differences were observed for the EAE parameters disease onset (EAE, 12.2 ± 0.3742 *vs* 1wk Cup/EAE, 10.8 ± 0.4899 d after immunization; p = 0.06) and maximum disease score (EAE, 2.7 ± 0.4673 vs 1 wk Cup/EAE, 2.5 ± 0.4183; p = 0.76) (Fig. 2 A).

In a next step, we analyzed the forebrains of treated mice at distinct rostral-to-caudal levels for the presence and localization of PVCs, a hallmark of active MS lesions (Maggi et al., 2014). This analysis was performed at the level of the anterior commissure (i.e., R215-235), the ventral hippocampal commissure (i.e., R245-265) and the rostral hippocampus (i.e., R275-295), respectively. As shown in Fig. 2B/C, PVCs were virtually absent in the forebrains of control mice. Some infiltrates were found in the forebrains of MOG_{35-55}-immunized animals, and these were located predominantly around the third ventricle. In contrast, the forebrains of 1wk Cup/EAE animals contained a significant number of PVCs. Such infiltrates were widespread within the forebrain, including the cortex, CC, and subcortical regions.

Next, we examined whether the severity of cuprizone-induced injury (i.e., oligodendrocyte degeneration and microglia activation) correlates with the extent of peripheral immune cell recruitment. To investigate this aspect, two separate cohorts of animals were treated cuprizone for one or three weeks. A third cohort of animals was treated cuprizone for three weeks, followed by two weeks on normal chow (i.e., 3 weeks cuprizone + 2 weeks normal chow; 3 + 2) as published previously (see Fig. 3A) (Scheld et al., 2016; Ruther et al., 2017). First, we investigated myelination and microglia activation before the MOG_{35-55} immunization (see arrows in Fig. 3A which illustrates the time point of this analysis). As shown in Fig. 3B, demyelination (PLP and LFB/PAS) of the corpus callosum was absent in 1 week, moderate in 3 weeks, but severe in 3 + 2 weeks intoxicated animals, respectively. Concomitant to the extent of demyelination, microgliosis (IBA1) was moderate at 1 week, intermediate at week 3, and severe in 3 + 2 weeks intoxicated animals. Next, additional animals were immunized with MOG_{35-55} peptide after week 1, 3 or 3 + 2 cuprizone, and numbers of PVCs were quantified two weeks after the immunization with the MOG_{35-55} peptide. As demonstrated in Fig. 3C, the greater the extent of cuprizone-induced metabolic injury, the higher the number of PVCs. Numbers of PVCs per brain section were low in 1 week cup/EAE, intermediate in 3 weeks cup/EAE, and high in 3 + 2 weeks normal chow/EAE mice.

The resultant inflammatory foci were subsequently characterized at the level of the anterior commissure (i.e., R215) in the 1wk Cup/EAE animals. As shown in Fig. 4, these focal inflammatory infiltrates are characterized by perivascular immune cell accumulation (i.e., within an enlarged Virchow-Robin space; Fig. 4A/A'; H&E), perivascular microgliosis/infiltrating macrophages (Fig. 4B/B'; IBA1), and moderate demyelination (Fig. 4C/C'; LFB/PAS). Double staining experiments for CD3 (green) and GFAP (red) showed that lymphocytes progressed through the astrocytic *glia limitans perivascularis* to invade the surrounding neuropil (Fig. 4D; see arrowhead). Although anti-GFAP immunoreactivity principally increased around the lesions (Fig. 4E), the staining intensity was lost especially in perivascular regions with high immune cell density (Fig. 4F). Similar observations were made, if astrocytes were visualized with anti-ALDH1L1 antibodies (data not shown). To examine the presence of acute axonal injury around inflammatory infiltrates, we identified lesions in H&E-stained slides and stained adjacent sections with anti-APP antibodies, a marker for acute axonal injury (Hoflich et al., 2016). The density of APP$^+$ spheroids was assessed in concentric areas around the vessel centers. As shown in Fig. 4G/H, spheroid densities were highest in the immediate vicinity of the vessel and progressively declined with increasing distance. In summary, our results demonstrate that in the applied animal model oligodendrocyte apoptosis with concomitant microglia activation is sufficient to trigger peripheral immune cell recruitment into the forebrain after MOG_{35-55} immunization.

We next aimed to identify the factors linked to peripheral immune cell recruitment in the cuprizone model. Total mRNA samples from the CC of control mice and mice intoxicated with cuprizone for 1 week were analyzed using Affymetrix GeneChip® arrays. When a threshold of 1.5-fold regulation (control *versus* cuprizone) was applied, the expression of 344 probe sets was significantly up-regulated, whereas the expression of 227 probe sets genes was significantly reduced. As shown in Fig. 5A/B, 2D principal components analysis (PCA) clearly revealed similarities between the individual samples (i.e., the formation of clusters), demonstrating the reliability of the experiment. For a better interpretation of our gene expression data, Fig. 5C shows a heatmap (each column: one individual animal), where red represents up-regulated genes and blue represents down-regulated genes in cuprizone-intoxicated *versus*

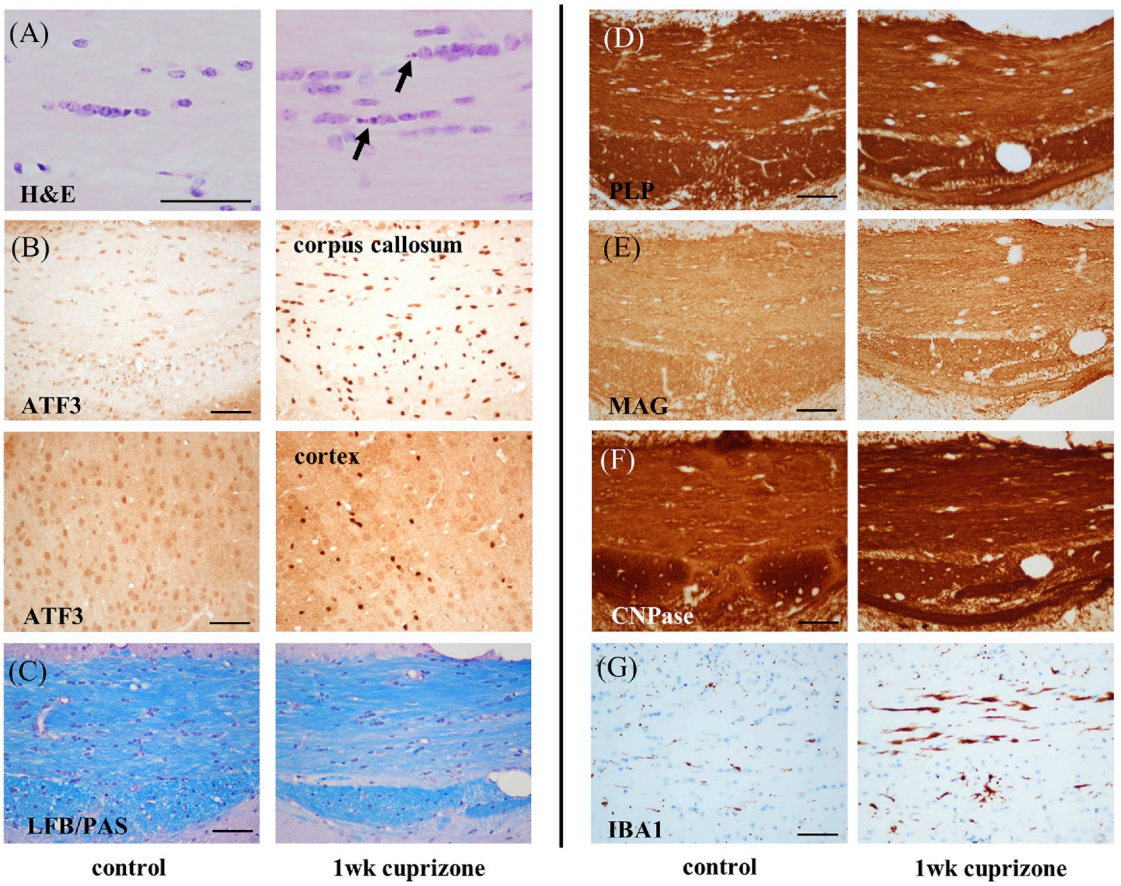

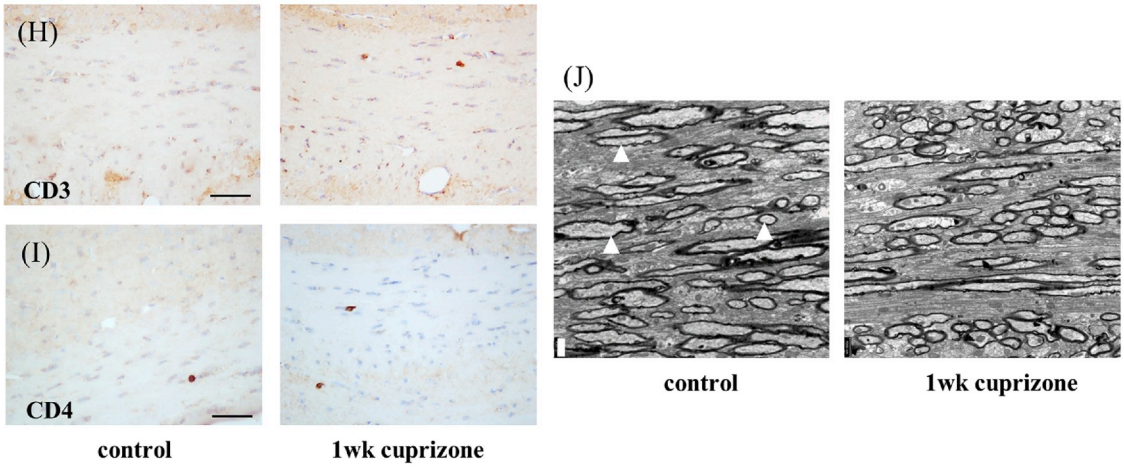

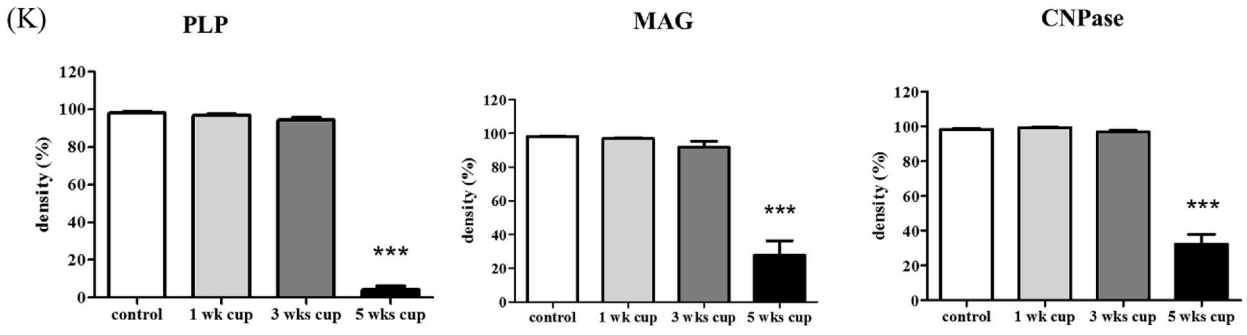

(caption on next page)

Fig. 1. Histopathological characteristics of the 1 week cuprizone lesion. (A) Representative H&E-staining to visualize apoptotic cells (arrows). (B) Anti-activating transcription factor 3 (ATF3) expression in the corpus callosum (CC) (upper row) and cortex (lower row) to demonstrate stressed oligodendrocytes. (C) Luxol fast blue (LFB)/periodic acid-Schiff (PAS) stain, (D) anti-proteolipid protein (myelin) 1 (PLP), (E) anti-myelin-associated glycoprotein (MAG) and (F) anti-2′,3′-cyclic nucleotide 3′ phosphodiesterase (CNPase) stain to demonstrate the myelination status of the corpus callosum. (G) Anti-ionized calcium-binding adapter molecule (IBA1) stain to demonstrate microglia activation. (H) Anti-CD3 and (I) anti-CD4 stain to demonstrate absence of T-lymphocytes in the CC. (J) Representative electron-microscopy images to demonstrate intact myelination on the ultrastructural level. Arrowheads indicate myelinated axons. (K) Quantification of anti-myelin proteins densities (i.e., anti-PLP, anti-MAG and anti-CNPase) of control, 1 week (wk), 3 wks, and 5 wks cuprizone (cup) animals (n = 4–5 per group). Statistical comparison was done using a one-way ANOVA with the obtained p-values corrected for multiple testing using the Dunnett's post hoc test. Significant differences with respect to the control animals are indicated by ***$p < 0.001$. (A) Scale bar: 25 μm. (B–I) Scale bar: 50 μm. (J) Scale bar: 1000 nm.

control animals. Black represents unchanged gene expression levels. As demonstrated, the expression of well-known oligodendrocyte specific genes, such as *Mag* (myelin associated glycoprotein), *Mal* (myelin and lymphocyte protein), *Aspa* (aspartoacylase) or *Mog* (myelin oligodendrocyte glycoprotein) was significantly reduced after 1 week of cuprizone intoxication (lower-right cluster in Fig. 5C). In contrast, the expression of chemokines which have been shown to be induced during the course of cuprizone-induced demyelination, such as *Cxcl0* (Clarner et al., 2015) or *Ccl3* (Janssen et al., 2016) showed higher expression levels (upper-right cluster). For a complete list of up- and down-regulated genes see supplementary table 2. Next, we performed a gene ontology enrichment analysis with the detected down- and up-regulated genes, respectively. Computing genes for which expression was found to be down-regulated revealed greatest enrichments for the biological process terms 'central nervous system myelination' (28.5-fold enrichment), 'cholesterol biosynthetic process' (20.5-fold enrichment), 'Schwann cell differentiation' (16.2-fold enrichment), and 'regulation of gliogenesis' (7.5-fold regulation). Computing genes for which expression was found to be up-regulated revealed greatest enrichments for the biological process terms 'antigen processing and presentation of exogenous peptide antigen via MHC class I' (51.9-fold enrichment), 'positive regulation of tumor necrosis factor biosynthetic process' (29.9-fold enrichment), 'MyD88-dependent toll-like receptor signaling pathway' (24.3-fold enrichment), and 'response to interferon-alpha' (22.7-fold regulation). This result further supports our hypothesis that cuprizone-induced oligodendrocyte injury activates pathways which are involved in the local (re-) activation of peripheral immune cells (see supplementary table 2 for a complete list of genes and expression values).

One of the genes which displayed high expression induction was moesin (*Msn*). This protein belongs to the ezrin-radixin-moesin (ERM) family of proteins, which plays structural and regulatory roles in the rearrangement of plasma membrane flexibility and protrusions through interaction with cortical actin filaments and the plasma membrane (Pore and Gupta, 2015). Since it has been reported that moesin is expressed in microglia/macrophages (Moon et al., 2011; Kashimoto et al., 2013), and microglia activation is one characteristic feature of early cuprizone lesions, we focused on this particular ERM-protein.

To verify our gene array data, and to visualize which cell type(s) express moesin, brain slides from control and 1 week cuprizone-intoxicated mice were processed for immunohistochemistry. As shown in Fig. 6A–C, low densities of moesin$^+$ cells were found in the CC and cortex of control animals. Moesin$^+$ cells showed morphological characteristics of either endothelial cells (Berryman et al., 1993) (arrow in Fig. 6B' and insert which shows a CD34/moesin double-stain) or microglia (arrow in Fig. 6C'). Densities of moesin$^+$ cells were higher in both brain regions after 1 week cuprizone intoxication (Fig. 6D/E). To verify that the non-endothelial, moesin$^+$ cell population belongs to the microglia cell lineage, adjacent sections were processed for IBA1/moesin immunofluorescence double staining experiments. As demonstrated in Fig. 6 F/G, there was a clear co-localization of the anti-moesin and anti-IBA1 signal. Blinded evaluation revealed that virtually all moesin$^+$ cells co-express IBA1 (data not shown). Furthermore, CD3/moesin immunofluorescence double staining experiments showed that lymphocytes expressed moesin as well (Fig. 6H).

Finally, we analyzed moesin expression in the brains of MS patients. In normal appearing grey matter tissues (i.e., no evidence of demyelination), moesin was prominently localized to structures what appeared to be endothelial cells (arrowhead in Fig. 7A/B). Occasionally glial cells, possibly microglia, were moesin immunoreactive (see arrow in Fig. 7B). No apparent immunoreactivity was detected in what appeared to be neurons. Comparable to what we found in the cortex, structures what appeared to be endothelial cells and microglia cells were moesin$^+$ in the normal appearing white matter (NAWM). Of note, the used antibody recognized the fine processes of scattered microglia (see arrow in Fig. 7C). Next, we analyzed moesin expression in six different MS lesions (i.e., three chronic active and three chronic inactive lesions). A representative chronic active lesion is shown in Fig. 7D–F and H. On the histopathological level, this lesion is characterized by focal demyelination (Fig. 7D/E), and accumulation of MHC-II$^+$ microglia/monocytes particularly at the rim of the lesion (Fig. 7F/G). A high density of moesin$^+$ cells was observed at the rim of chronic active MS lesions (Fig. 7I). Furthermore, as shown in Fig. 7J, moesin$^+$ cells were observed in enlarged perivascular spaces, indicating that peripheral immune cells express moesin in MS as well. Slightly reduced densities of moesin$^+$ cells were found in the NAWM (Fig. 7K) and inactive lesion areas such as the center of chronic inactive lesions (Fig. 7L). Blinded quantification of moesin$^+$ cells in three chronic active lesions revealed lowest densities in the NAWM, and highest densities within the active lesion areas (Fig. 7N; $p = 0.1042$). MHC-II/moesin immunofluorescence double staining experiments (Fig. 7M) verified that virtually all MHC-II$^+$ cells express moesin. However, not all moesin$^+$ cells were MHC-II$^+$ (~88%), suggesting that moesin stains both activated and non-activated microglia/macrophages and endothelial cells.

4. Discussion

Here, we describe that early cuprizone lesions, which are characterized by oligodendrocyte apoptosis and microglia activation, trigger peripheral immune cell recruitment into the forebrain after MOG_{35-55} immunization. On the one hand, this study clearly illustrates the significance of brain-intrinsic degenerative cascades for immune cell recruitment and, possibly, MS lesion formation. On the other hand, our findings add to the understanding of the Cup/EAE model, a practical and effective tool for studying immune cell recruitment into the forebrain. Of note, the model has great translational potential, as most imaging and pathological MS studies are performed in the forebrain. By contrast, most EAE studies focus on spinal cord tissues.

Pathological changes associated with the formation of new inflammatory MS lesions are difficult to study, because such lesions are rarely fatal. Two main strategies can be pursued to understand underlying mechanisms of MS lesion formation: (i) To describe pathological findings in patients who died relatively early after the onset of a new symptomatic lesion, or (ii) to investigate brain biopsies of patients diagnosed with tumefactive MS, also called "pseudotumoral MS", a well-recognized variant of MS (Hardy et al., 2016; Totaro et al., 2016). Following the first approach, Barnett and Prineas reported that the earliest pathological changes, described as prephagocytic lesions, consist of oligodendrocyte apoptosis and microglial activation associated with few lymphocytes and phagocytes in regions of relative myelin preservation. This was reported to be followed by the disappearance of oligodendrocytes and the presence of intramyelinic edema with tissue

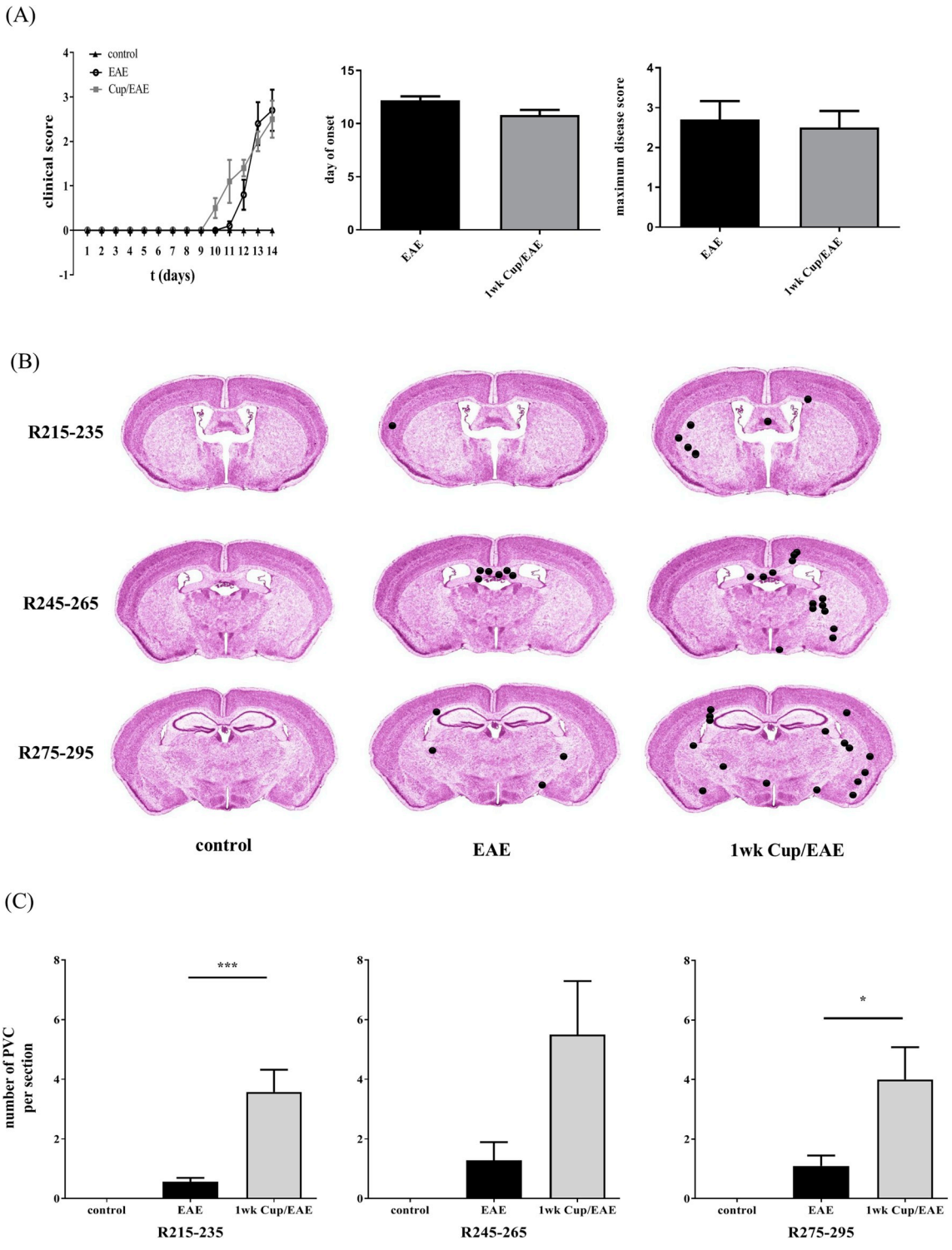

Fig. 2. Clinical disease progression and forebrain inflammatory cell infiltration. (A) Clinical scores of control, experimental autoimmune encephalomyelitis (EAE) and 1wk cuprizone/EAE (1wk Cup/EAE) mice. Five animals per experimental group, one representative experiment. The left image shows the progression of clinical disease in the three different cohorts of mice. The center image shows the mean day of disease onset of EAE and 1wk Cup/EAE mice. The right image shows the mean maximum disease score of EAE and 1wk Cup/EAE mice. Comparison of the mean day of disease onset and maximum disease score were done using unpaired *t*-test. (B) Distribution of perivascular cuffs (PVCs) in the different treatment groups (H&E staining; black dots from one independent observer) at three brain levels (regions according to Sidman et al.). (C) Quantification of the number of PVCs at three distinct brain levels. At R215-235, 33 slides were analyzed in control animals (n = 4), 44 slides in EAE animals (n = 5), and 40 slides in 1wk Cup/EAE animals (n = 5). At R245-265, 7 slides were analyzed in control animals (n = 4), 7 slides in EAE animals (n = 5), and 8 slides in 1wk Cup/EAE animals (n = 5). At R275-295, 8 slides were analyzed in control animals (n = 4), 10 slides in EAE animals (n = 5), and 8 slides in 1wk Cup/EAE animals (n = 5). Comparison of the numbers of PVCs was done using one-way ANOVA with the obtained p-values corrected for multiple testing using the Tukey's post hoc test. Significant differences in between the three experimental groups are indicated by *$p < 0.05$, **$p < 0.01$, or ***$p < 0.001$.

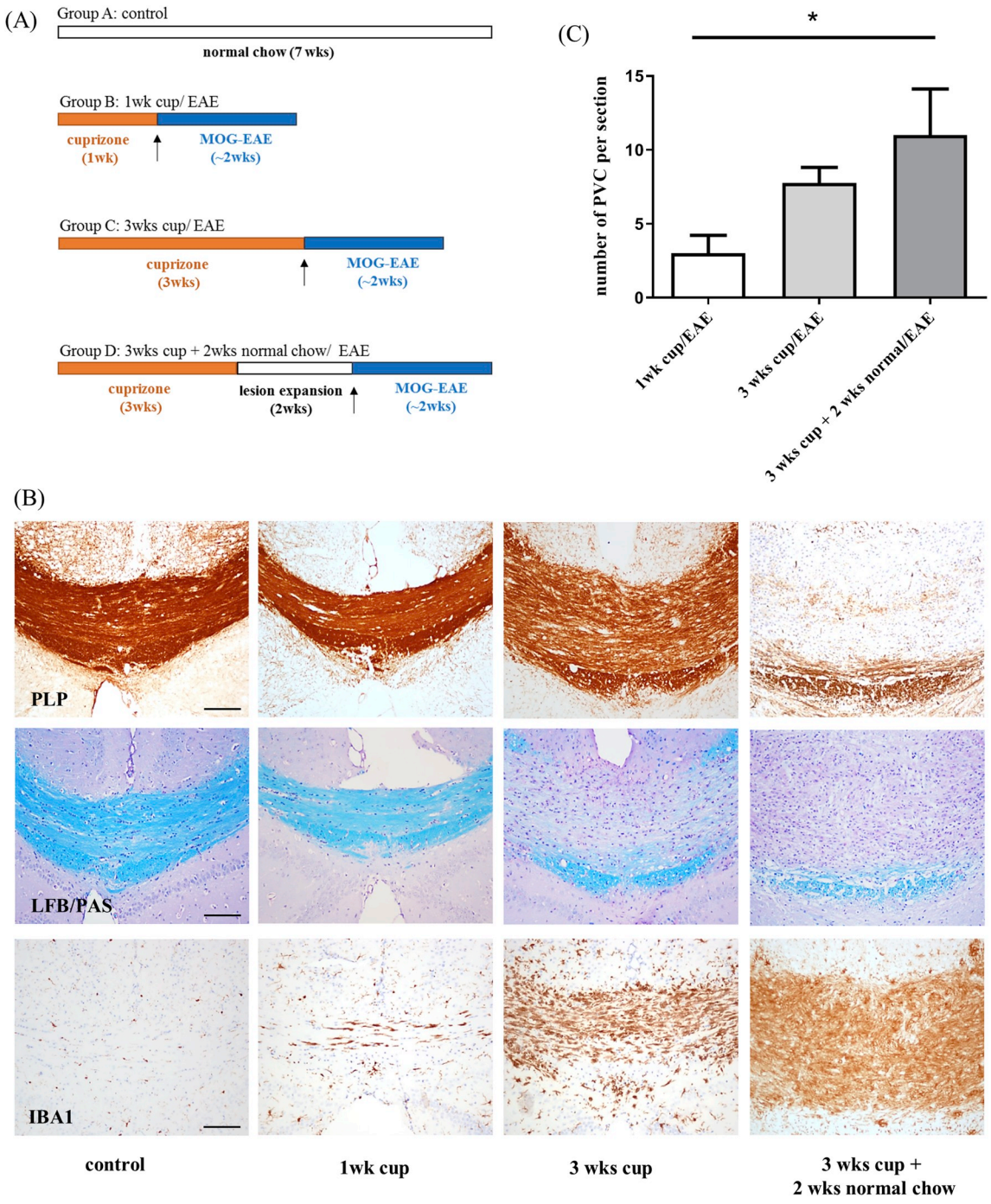

Fig. 3. Correlation between severity of demyelination and forebrain inflammatory cell infiltration. (A) Schematic depicting the experimental setup. (B) Anti-proteolipid protein (myelin) 1 (PLP)-stain (upper-row), Luxol fast blue (LFB)/periodic acid-Schiff (PAS) stain (middle-row) and anti-ionized calcium-binding adapter molecule-stain (lower-row, IBA1) to demonstrate demyelination and concomitant microgliosis of the corpus callosum. Animals were subjected to a 1 week or 3 weeks continuous cuprizone intoxication protocol. One additional group was intoxicated with cuprizone for 3 weeks, followed by 2 weeks on normal chow before scarification. (C) Quantification of the number of perivascular cuffs (PVCs) per section at the level R215 in 1wk Cup/EAE (n = 9), 3wks Cup/EAE (n = 8) or 3 wks followed by 2 wks on normal chow/EAE (n = 5) mice. Comparison of the numbers of PVCs per section was done using one-way ANOVA with the obtained p-values corrected for multiple testing using the Tukey's post hoc test. Significant differences in between the three experimental groups are indicated by *$p < 0.05$. (A) Scale bar: 100 μm.

vacuolization. Finally, the myelin sheaths were fragmented and phagocytosed by macrophages in the presence of infiltrating T cells (Barnett and Prineas, 2004). The earliest steps during the evolution of new, inflammatory lesions was, therefore, oligodendrocyte stress, paralleled by microglia activation. Similar observations were reported by others. For example, De Groot and colleagues subjected unfixed post-mortem brain slices to T(1)- and T(2)-weighted magnetic resonance imaging, followed by macroscopic and microscopic examination of the tissues. The authors described so-called 'preactive' lesions and speculated that this lesion type might represent one of the earliest stages during MS lesion development (De Groot et al., 2001). Preactive lesions were observed throughout the normal-appearing white matter and were characterized by clustering of activated microglia in the absence of overt demyelination (van der Valk and De Groot, 2000). The presence

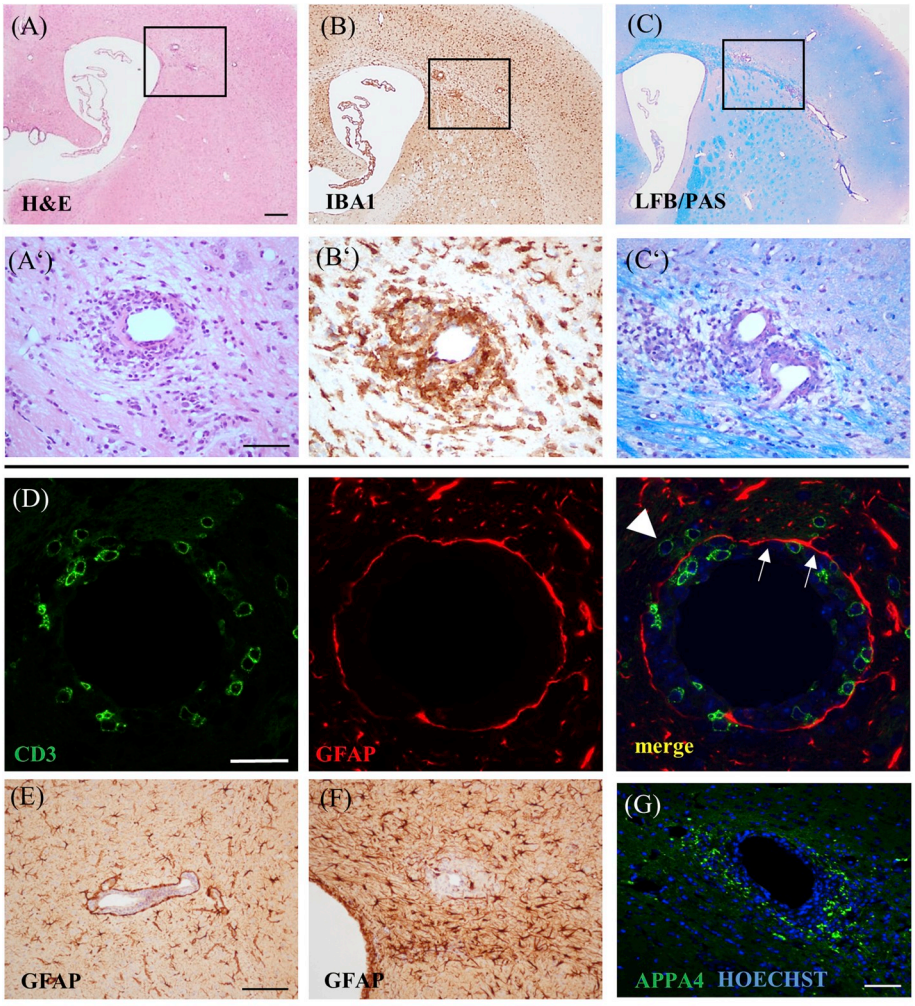

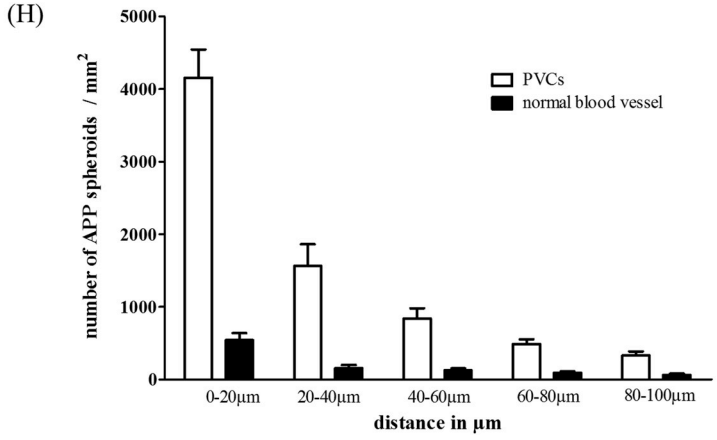

Fig. 4. Forebrain inflammatory cell infiltration and acute axonal injury. Representative perivascular cuffs (PVCs) of a 1wk Cup/EAE mouse at R225 (see Fig. 3 for grouping). (A/A′) H&E staining to demonstrate a perivascular lesions in which most immune cells are trapped in the enlarged perivascular space. (B/B′) Anti-ionized calcium-binding adapter molecule (IBA1) stain to demonstrate perivascular microglia and monocyte accumulation. (C/C′) Luxol fast blue (LFB)/periodic acid-Schiff (PAS) stain to demonstrate partial demyelination around a perivascular lesion where immune cells invaded the neuropil. (D) Anti- CD3 and anti-glial fibrillary acidic protein (GFAP) double stain to demonstrate migration of lymphocytes over the *glia limitans perivascularis* into the surrounding neuropil. Arrows indicate the *glia limitans perivascularis* whereas the arrowhead indicates a $CD3^+$ lymphocyte in the perivascular neuropil. (E/F) Anti-GFAP stain to demonstrate astrocyte pathology around PVCs. (G) Anti-amyloid beta (A4) precursor protein (APP) stain to demonstrate acute axonal injury in perivascular areas as spheroids. Counterstaining with Hoechst 33258 (blue) to show the cell nuclei. (H) APP^+ spheroid densities were quantified in concentric areas (up to 100 µm) from the vessel center. Inflamed (white columns) and normal vessels (black columns) were included. For each sector, 25 perivascular regions with and without lesions (5–6 animals) were analyzed. (A–C) Scale bar: 250 µm. (A′-C′, G) Scale bar: 50 µm. (D) Scale bar: 25 µm. (E–F) Scale bar: 100 µm.

of stressed oligodendrocytes in these preactive lesions was reported later (van Noort et al., 2010) while van Horssen et al. (2012) showed that the preactive lesions were not associated with blood-brain barrier disruption, suggesting that an intrinsic trigger of innate immune activation, rather than extrinsic factors crossing a damaged blood-brain barrier, induces the formation of clusters of activated microglia (van Horssen et al., 2012). In another study, Marik and colleagues found abundant areas of microglial activation in the absence of detectable demyelination in human MS autopsy tissues. Such areas of microglial activation were localized in a broad zone surrounding the border of actively demyelinating lesions, and less frequently also presented as separate lesions, which occurred independently from actively demyelinating plaques (Marik et al., 2007). Of note, such 'pre-demyelinating' lesions were specific for pattern III demyelination, in which oligodendrocyte apoptosis is a major characteristic (Lucchinetti et al., 2000). The authors suggested that focal areas of microglial activation may precede the formation of demyelinating plaques in MS patients exhibiting hypoxia-like, pattern III demyelination. Comparably, Henderson and colleagues demonstrated that early loss of oligodendrocytes along with macrophage activation is a prominent feature in tissues bordering rapidly expanding MS lesions. Of note, parenchymal lymphocytes were largely absent in such areas (Henderson et al., 2009). In

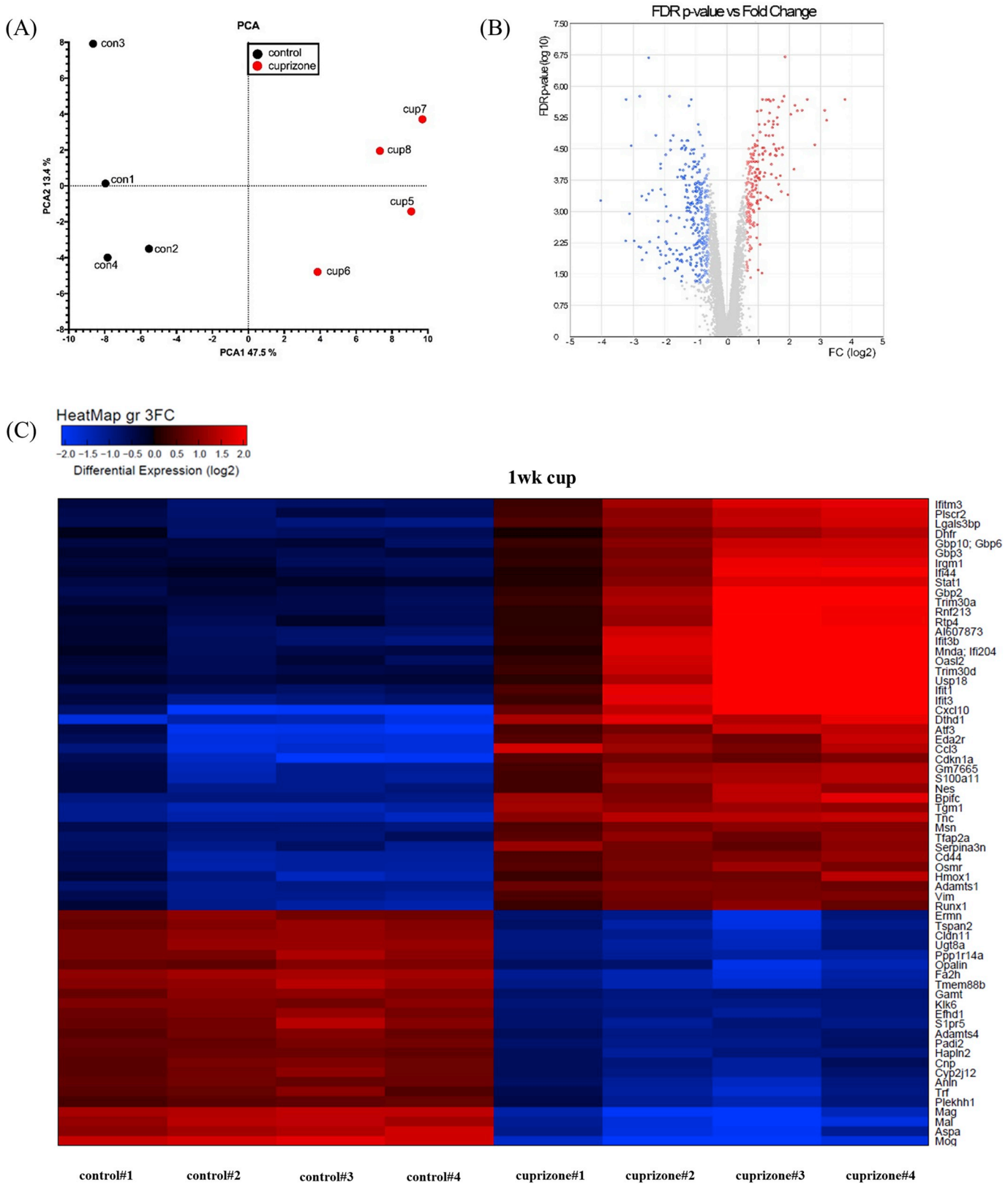

Fig. 5. (A) Principal component 2D-analysis (PCA) of the gene expression data set. Each dot represents a corpus callosum sample. (B) Volcano plot of differentially abundant transcripts. (C) Heatmap in which genes have been grouped based on their pattern of gene expression. Each column represent one individual animal (control: 4 animals; 1 week cuprizone: 4 animals). The color and intensity of the boxes is used to represent changes (not absolute values) of gene expression. Red represents up-regulated genes and blue represents down-regulated genes. Black represents unchanged expression. Only genes significantly (FDR p-value < 0.05) differentially expressed with a minimal change in expression by 3-fold are illustrated.

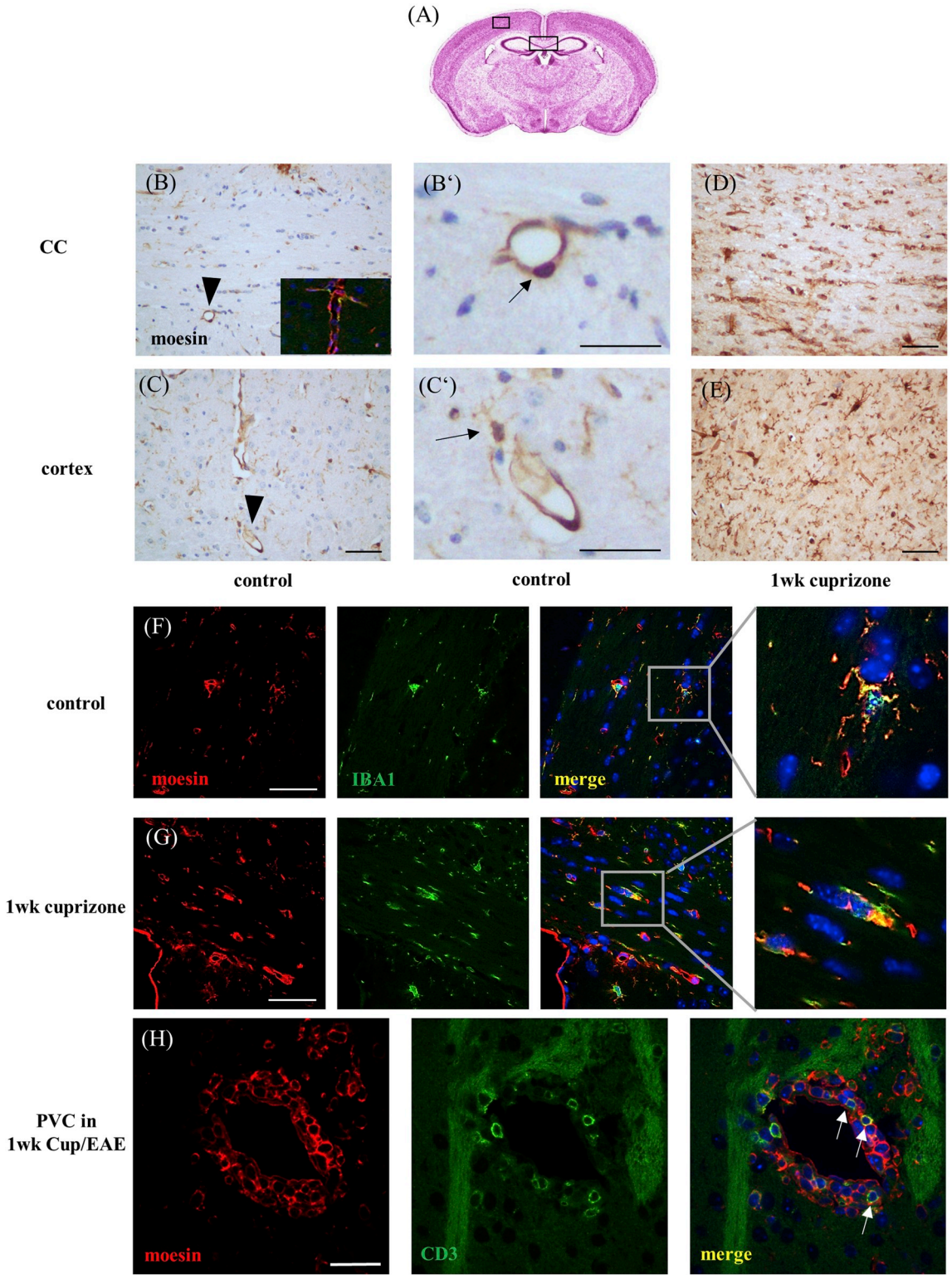

Fig. 6. Moesin expression in the cuprizone model. (A) Schematic depicting the two principal regions (according to Sidman et al.) included in this part of the study, namely the midline of the corpus callosum (CC) (big box) and the primary somatosensory cortex area (small box). (B/B′) Representative anti-moesin stain of the CC in control animals. Insert in (B) shows a representative immunofluorescence double staining against CD34 (endothelial marker; green) and moesin (red). The vessel shown in (B) by the arrowhead is shown in B′ in higher magnification. (C/C′) Representative anti-moesin stain of the somatosensory cortex area in control animals. The vessel shown in (C) by the arrowhead is shown in C′ in higher magnification. The arrow in C′ highlights a moesin$^+$ microglia cell. Anti-moesin stain of the corpus callosum (D) and somatosensory cortex area (E) after 1 week cuprizone-intoxication. (F/G) Anti-ionized calcium-binding adapter molecule (IBA1)/anti-moesin immunofluorescence double stain in control (F) and 1 week cuprizone-intoxicated mice (G). Note that moesin is expressed by IBA1$^+$ microglia. (H) Anti-moesin/anti-CD3 immunofluorescence double stain in 1wk Cup/EAE mice. Note that moesin is expressed by CD3$^+$ lymphocytes (arrows). (B–F) Scale bar: 50 µm. (B'/C'/H) Scale bar: 25 µm.

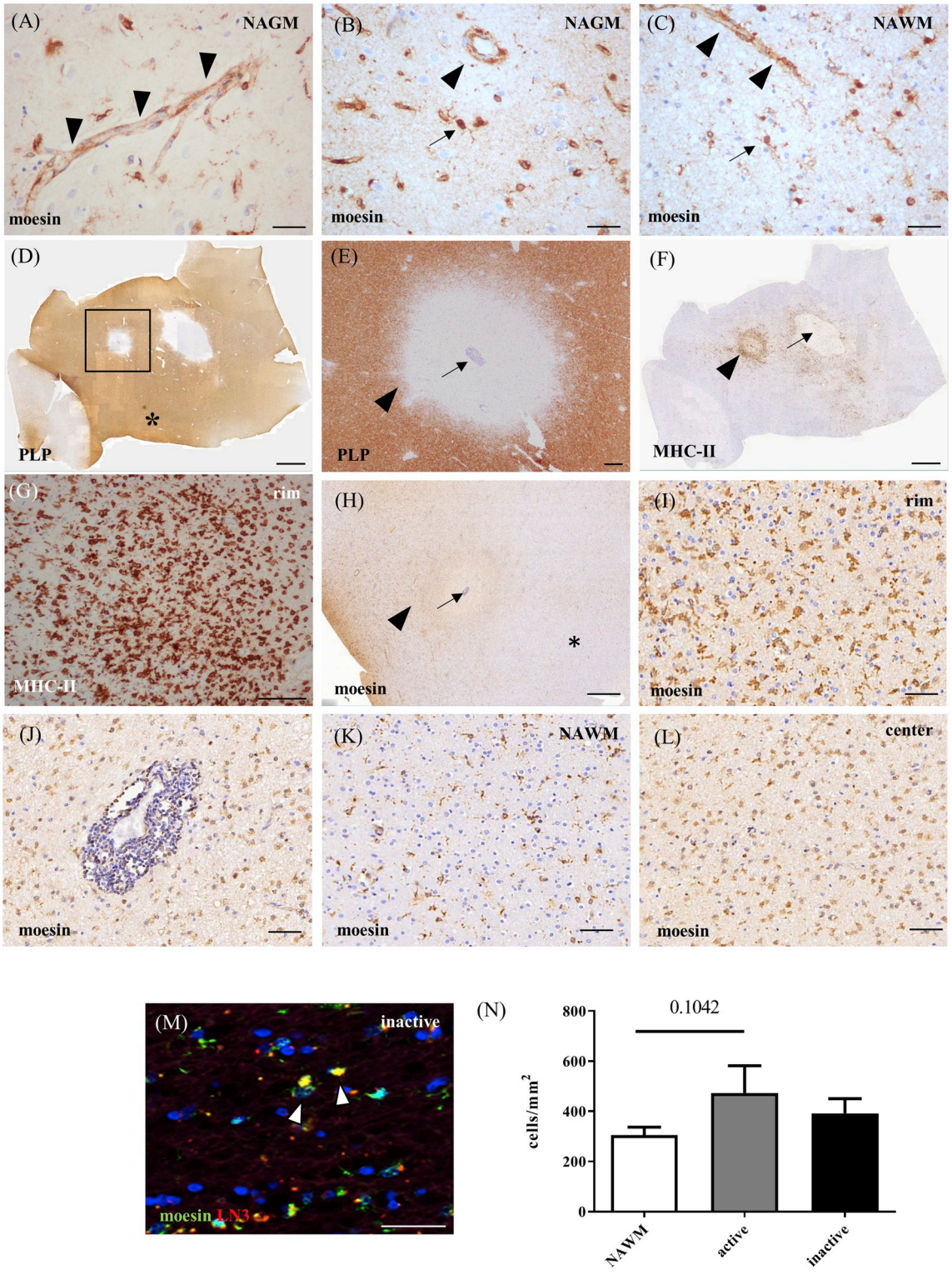

Fig. 7. Moesin expression in multiple sclerosis lesions. (A/B) Representative anti-moesin stains of the normal appearing grey matter (NAGM). Arrowheads highlight a moesin$^+$ blood vessel, the arrow highlights a moesin$^+$ microglia. (C) Representative anti-moesin stain of the normal appearing white matter (NAWM). Arrowheads highlight a moesin$^+$ blood vessel, the arrow highlights a moesin$^+$ microglia. (D) Representative anti-proteolipid protein (myelin) 1 (PLP)-stain of a chronic active lesion. Area highlighted by the box is shown in (E) in higher magnification. The star in (D) indicates NAWM. (E) The arrow highlights the center of the lesion with an inflamed vessel, the arrowhead highlights the border of the lesion. (F) Representative anti-MHC class II stain of the same section as shown in (D). The arrow highlights an inactive lesion center, the arrowhead highlights an active lesion border, which is shown in (G) in higher magnification. (H) Representative anti-moesin stain of the same section as shown in (D). The arrow highlights an inactive lesion center, the arrowhead highlights an active lesion border, the star highlights the NAWM. Moesin$^+$ cells are found at high densities at the rim of the chronic-active lesion (I) and within enlarged perivascular spaces (J). Lower densities of moesin$^+$ cells can be seen in the NAWM (K) and the inactive lesion center (L). (M) MHC-II/moesin immunofluorescence double staining of a chronic active lesion. (N) Quantification of moesin$^+$ cell densities in the normal appearing white matter (NAWM), center and border of chronic active MS lesions. Mann-Withney test was performed to compare differences between the groups. (A–C) Scale bar: 40 µm. (D/F) Scale bar: 2 mm. (E) Scale bar: 150 µm. (G, I, J, K, L) Scale bar: 50 µm. (H) 300 µm. (M) Scale bar: 50 µm.

another study using EAE in marmosets, Maggi and colleagues compared serial *in vivo* magnetic resonance imaging (MRI) to postmortem tissues. Here the authors show that early inflammatory lesions in EAE are characterized by focal microglia and astrocyte activation in the absence of demyelination and parenchymal lymphocytes (Maggi et al., 2014). Likewise, in MS, serial MRI studies have shown that focal changes in the normal appearing white matter are present at locations that later develop into focal T2 lesions that enhance with gadolinium (Filippi et al., 1998; Narayana et al., 1998). Such MRI studies have revealed that MS lesions are initiated several days or weeks before the appearance of the classical inflammatory demyelinating plaque (Filippi et al., 1998; Narayana et al., 1998) indicating that the blood-brain barrier appears to be intact at the earliest stages of lesion development.

Taken together, all these findings suggest a key role for brain intrinsic pathological processes during the earliest stages of MS lesion formation, and that areas of microglia activation precede the full-fledged inflammatory demyelination. Here, we demonstrate that several histopathological characteristics of early MS lesions are reproduced by a short-term cuprizone intoxication protocol, *id est* oligodendrocyte stress, focal microglia activation, absence of lymphocytes and absence of overt demyelination (see Fig. 1). These findings are in line with previous reports (Buschmann et al., 2012; Hagemeier et al., 2013; Clarner et al., 2015). In the present study, oligodendrocyte stress was detected by either the visualization of apoptotic bodies or the presence of ATF3$^+$ cells. Also not formally proven in the current study, we previously reported that activated caspase 3-expressing cells are found in close vicinity to CNPase-reactive fibers after short-term cuprizone intoxication (Buschmann et al., 2012), and that ATF3-expressing cells co-express the oligodendrocyte marker protein CC-1 (Goldberg et al., 2013). The presence of apoptotic cells in the CC of cuprizone-intoxicated mice has been well reported by other groups (Acs and Komoly, 2012; Hagemeier et al., 2013). Comparably, early microglia activation after short-term cuprizone intoxication has also been reported by us and other groups (Hagemeier et al., 2013; Clarner et al., 2015; Krauspe et al., 2015). Our studies thus support the finding that early cuprizone lesions are characterized by oligodendrocyte stress which leads to oligodendrocyte degeneration and concomitant microglia activation. Of note, whether minor demyelination is present in such early lesions remains to be clarified in future studies.

How this relatively mild pathological process triggers peripheral immune cell recruitment is currently unclear. Early studies in the sixties showed that many focal CNS injuries can principally trigger the formation of EAE lesions in these damaged areas. This has been shown for electrical or thermal burns (Clark and Bogdanove, 1955; Bogdanove and Clark, 1957; Levine and Hoenig, 1968), implantation of chemicals (Levine et al., 1963), or anoxic injuries (Levine and Wenk, 1967). The gene array analyses conducted in this study revealed that cuprizone-induced oligodendrocyte apoptosis is paralleled by expression induction of genes known to regulate the cytoskeletal network. One of these induced proteins is moesin. Moesin, a **m**embrane-**o**rganizing **e**xtension **s**pike prote**in**, belongs to the ezrin/radixin/moesin family of proteins distributed in the plasma membrane in the cellular cortex. Collectively, these three proteins are also known as the ERM protein family. Under physiological conditions, microglial cells exhibit a highly ramified morphology characterized by motile processes that constantly monitor their immediate surrounding by extending and retracting their processes (Nimmerjahn et al., 2005). In case of a harmful event, the generation of effective immune responses by microglia necessitates their morphological transformation (or “activation”). During activation microglia cells retract their processes, and their cell bodies become hypertrophic. The ERM family proteins are in this context of particular interest as they orchestrate the assembly and stabilization of plasma membrane interactions through their ability to interact with transmembrane proteins and the cytoskeleton (Fehon et al., 2010). In doing so, they provide structural links to strengthen the cell cortex and facilitate several key cellular process, including the membrane dynamics, substrate adhesion, cell survival, determination of cell shape, polarity, formation of membrane protrusions, cell adhesion and motility (Pore and Gupta, 2015; Pines et al., 2017). In this study, we demonstrated that induction of moesin expression is a robust and early event in the cuprizone model. Immunofluorescence double labelling experiments showed that besides endothelial cells, moesin is expressed by IBA1$^+$ microglia. Furthermore, activated, LN3$^+$ microglia/monocytes express moesin in MS lesions. It has been shown that moesin is expressed by, and functionally active in endothelial cells (Berryman et al., 1993; Schwartz-Albiez et al., 1995; Vitorino et al., 2015). Expression and/or activation of moesin in microglia is less well appreciated, but microglia in the spinal cord were found to express moesin in a model of peripheral nerve injury (Kashimoto et al., 2013). Furthermore, it has been shown that microglia express moesin in cryogenic traumatic brain injury of the mouse cortex (Moon et al., 2011). In the latter study, moesin expression was also observed in resting microglia (Moon et al., 2011). In MS lesions we frequently found round, small moesin-expressing cells, reminiscent of lymphocytes and moesin$^+$ cells within the enlarged perivascular spaces of MS lesions (seeFig. 7I). At least in mice we can show that moesin expression is not restricted to monocytes, but can also be expressed by T cells (Schwartz-Albiez et al., 1995; Ansa-Addo et al., 2017). Of note, it has recently been shown that moesin controls differentiation of regulatory T cells (Ansa-Addo et al., 2017) and regulates lymphocyte trafficking (Nomachi et al., 2013). To our knowledge, this is the first report, demonstrating expression of moesin in MS lesions, however the function of moesin during lesion formation and progression is currently not known. Moesin knock-down animals develop normally and are fertile, with no obvious histological abnormalities in any of the tissues examined. Whether moesin deficient mice develop less severe demyelination in the cuprizone model, and whether these mice are protected from active EAE are unknown and may provide important information for lesion formation in MS.

As mentioned in the results section of this manuscript, the mRNA expression of well-known oligodendrocyte specific genes was significantly reduced after 1 week of cuprizone intoxication. However, we did not find any evidence of demyelination at week 1 on the histochemical and immunohistochemical level (see Fig. 1). In a recent paper we were able to demonstrate that cuprizone-induced oligodendrocyte apoptosis is paralleled by the activation of the endoplasmic-reticulum stress response (Fischbach et al., 2018). One component of the endoplasmic-reticulum stress response is the selective and regulated degradation of mRNA, termed regulated IRE1-dependent decay (RIDD), which relieves endoplasmic-reticulum stress by reducing the amount of the endoplasmic-reticulum protein load. We speculate that although myelin protein synthesis is reduced in the stressed oligodendrocytes, the myelin sheaths remain stable for several days or even weeks before demyelination is visible on the histological level.

In summary, this study indicates that oligodendrocyte degeneration and concomitant microglia activation might trigger peripheral immune cell recruitment in MS, and thus, the formation of focal inflammatory lesions. A better understanding of the underlying mechanisms would allow approaches to suppress the development of inflammatory MS lesions at their earliest stages.

Conflicts of interest

The authors declare no competing financial interests.

Acknowledgements

This study was supported by the Dr. Robert Pfleger Stiftung (M.K.) and the Deutsche Forschungsgemeinschaft (KI 1469/8-1). The technical support from P. Ibold, H. Helten, S. Wübbel, B. Aschauer, and A. Baltruschat is acknowledged.

Appendix A. Supplementary data

Supplementary data to this article can be found online at https://doi.org/10.1016/j.neuint.2019.03.005.

References

Acs, P., Kipp, M., Norkute, A., Johann, S., Clarner, T., Braun, A., Berente, Z., Komoly, S., Beyer, C., 2009. 17beta-estradiol and progesterone prevent cuprizone provoked demyelination of corpus callosum in male mice. Glia 57 (8), 807–814.

Acs, P., Komoly, S., 2012. Selective ultrastructural vulnerability in the cuprizone-induced experimental demyelination. Ideggyogy Sz. 65 (7–8), 266–270.

Ansa-Addo, E.A., Zhang, Y., Yang, Y., Hussey, G.S., Howley, B.V., Salem, M., Riesenberg, B., Sun, S., Rockey, D.C., Karvar, S., Howe, P.H., Liu, B., Li, Z., 2017. Membrane-organizing protein moesin controls Treg differentiation and antitumor immunity via TGF-beta signaling. J. Clin. Investig. 127 (4), 1321–1337.

Barnett, M.H., Prineas, J.W., 2004. Relapsing and remitting multiple sclerosis: pathology of the newly forming lesion. Ann. Neurol. 55 (4), 458–468.

Bauer, J., Rauschka, H., Lassmann, H., 2001. Inflammation in the nervous system: the human perspective. Glia 36 (2), 235–243.

Benn, T., Halfpenny, C., Scolding, N., 2001. Glial cells as targets for cytotoxic immune mediators. Glia 36 (2), 200–211.

Berryman, M., Franck, Z., Bretscher, A., 1993. Ezrin is concentrated in the apical microvilli of a wide variety of epithelial cells whereas moesin is found primarily in endothelial cells. J. Cell Sci. 105 (Pt 4), 1025–1043.

Bogdanove, L.H., Clark, G., 1957. The induction of exacerbations of allergic meningoencephalomyelitis. J. Neuropathol. Exp. Neurol. 16 (1), 57–60.

Buschmann, J.P., Berger, K., Awad, H., Clarner, T., Beyer, C., Kipp, M., 2012. Inflammatory response and chemokine expression in the white matter corpus callosum and gray matter cortex region during cuprizone-induced demyelination. J. Mol. Neurosci. 48 (1), 66–76.

Clark, G., Bogdanove, L.H., 1955. The induction of the lesions of allergic meningoencephalomyelitis in a predetermined location. J. Neuropathol. Exp. Neurol. 14 (4), 433–437.

Clarner, T., Diederichs, F., Berger, K., Denecke, B., Gan, L., van der Valk, P., Beyer, C., Amor, S., Kipp, M., 2012. Myelin debris regulates inflammatory responses in an experimental demyelination animal model and multiple sclerosis lesions. Glia 60 (10), 1468–1480.

Clarner, T., Janssen, K., Nellessen, L., Stangel, M., Skripuletz, T., Krauspe, B., Hess, F.M., Denecke, B., Beutner, C., Linnartz-Gerlach, B., Neumann, H., Vallieres, L., Amor, S., Ohl, K., Tenbrock, K., Beyer, C., Kipp, M., 2015. CXCL10 triggers early microglial activation in the cuprizone model. J. Immunol. 194 (7), 3400–3413.

De Groot, C.J., Bergers, E., Kamphorst, W., Ravid, R., Polman, C.H., Barkhof, F., van der Valk, P., 2001. Post-mortem MRI-guided sampling of multiple sclerosis brain lesions: increased yield of active demyelinating and (p)reactive lesions. Brain 124 (Pt 8), 1635–1645.

Fehon, R.G., McClatchey, A.I., Bretscher, A., 2010. Organizing the cell cortex: the role of ERM proteins. Nat. Rev. Mol. Cell Biol. 11 (4), 276–287.

Ferguson, B., Matyszak, M.K., Esiri, M.M., Perry, V.H., 1997. Axonal damage in acute multiple sclerosis lesions. Brain 120 (Pt 3), 393–399.

Filippi, M., Rocca, M.A., Martino, G., Horsfield, M.A., Comi, G., 1998. Magnetization transfer changes in the normal appearing white matter precede the appearance of enhancing lesions in patients with multiple sclerosis. Ann. Neurol. 43 (6), 809–814.

Fischbach, F., Nedelcu, J., Leopold, P., Zhan, J., Clarner, T., Nellessen, L., Beissel, C., van Heuvel, Y., Goswami, A., Weis, J., Denecke, B., Schmitz, C., Hochstrasser, T., Nyamoya, S., Victor, M., Beyer, C., Kipp, M., 2018. "Cuprizone-induced Graded Oligodendrocyte Vulnerability Is Regulated by the Transcription Factor DNA Damage-Inducible Transcript 3." Glia.

Goldberg, J., Daniel, M., van Heuvel, Y., Victor, M., Beyer, C., Clarner, T., Kipp, M., 2013. Short-term cuprizone feeding induces selective amino acid deprivation with concomitant activation of an integrated stress response in oligodendrocytes. Cell. Mol. Neurobiol. 33 (8), 1087–1098.

Grosse-Veldmann, R., Becker, B., Amor, S., van der Valk, P., Beyer, C., Kipp, M., 2016. Lesion expansion in experimental demyelination animal models and multiple sclerosis lesions. Mol. Neurobiol. 53 (7), 4905–4917.

Hagemeier, K., Lurbke, A., Hucke, S., Albrecht, S., Preisner, A., Klassen, E., Hoffmann, E., Cui, Q.L., Antel, J.J., Bruck, W., Klotz, L., Kuhlmann, T., 2013. Puma, but not noxa is essential for oligodendroglial cell death. Glia 61 (10), 1712–1723.

Haider, L., Fischer, M.T., Frischer, J.M., Bauer, J., Hoftberger, R., Botond, G., Esterbauer, H., Binder, C.J., Witztum, J.L., Lassmann, H., 2011. Oxidative damage in multiple sclerosis lesions. Brain 134 (Pt 7), 1914–1924.

Hardy, T.A., Tobin, W.O., Lucchinetti, C.F., 2016. Exploring the overlap between multiple sclerosis, tumefactive demyelination and Balo's concentric sclerosis. Mult. Scler. 22 (8), 986–992.

Henderson, A.P., Barnett, M.H., Parratt, J.D., Prineas, J.W., 2009. Multiple sclerosis: distribution of inflammatory cells in newly forming lesions. Ann. Neurol. 66 (6), 739–753.

Hoflich, K.M., Beyer, C., Clarner, T., Schmitz, C., Nyamoya, S., Kipp, M., Hochstrasser, T., 2016. Acute axonal damage in three different murine models of multiple sclerosis: a comparative approach. Brain Res. 1650, 125–133.

Iglesias, A., Bauer, J., Litzenburger, T., Schubart, A., Linington, C., 2001. T- and B-cell responses to myelin oligodendrocyte glycoprotein in experimental autoimmune encephalomyelitis and multiple sclerosis. Glia 36 (2), 220–234.

Irizarry, R.A., Hobbs, B., Collin, F., Beazer-Barclay, Y.D., Antonellis, K.J., Scherf, U., Speed, T.P., 2003. Exploration, normalization, and summaries of high density oligonucleotide array probe level data. Biostatistics 4 (2), 249–264.

Janssen, K., Rickert, M., Clarner, T., Beyer, C., Kipp, M., 2016. Absence of CCL2 and CCL3 ameliorates central nervous system grey matter but not white matter demyelination in the presence of an intact blood-brain barrier. Mol. Neurobiol. 53 (3), 1551–1564.

Kashimoto, R., Yamanaka, H., Kobayashi, K., Okubo, M., Yagi, H., Mimura, O., Noguchi, K., 2013. Phosphorylation of ezrin/radixin/moesin (ERM) protein in spinal microglia following peripheral nerve injury and lysophosphatidic acid administration. Glia 61 (3), 338–348.

Konno, H., Yamamoto, T., Suzuki, H., Yamamoto, H., Iwasaki, Y., Ohara, Y., Terunuma, H., Harata, N., 1990. Targeting of adoptively transferred experimental allergic encephalitis lesion at the sites of wallerian degeneration. Acta Neuropathol. 80 (5), 521–526.

Kornek, B., Storch, M.K., Weissert, R., Wallstroem, E., Stefferl, A., Olsson, T., Linington, C., Schmidbauer, M., Lassmann, H., 2000. Multiple sclerosis and chronic autoimmune encephalomyelitis: a comparative quantitative study of axonal injury in active, inactive, and remyelinated lesions. Am. J. Pathol. 157 (1), 267–276.

Krauspe, B.M., Dreher, W., Beyer, C., Baumgartner, W., Denecke, B., Janssen, K., Langhans, C.D., Clarner, T., Kipp, M., 2015. Short-term cuprizone feeding verifies N-acetylaspartate quantification as a marker of neurodegeneration. J. Mol. Neurosci. 55 (3), 733–748.

Lake, J., Weller, R.O., Phillips, M.J., Needham, M., 1999. Lymphocyte targeting of the brain in adoptive transfer cryolesion-EAE. J. Pathol. 187 (2), 259–265.

Levine, S., 1960. Localization of allergic encephalomyelitis in lesions of cyanide encephalopathy. J. Neuropathol. Exp. Neurol. 19, 238–247.

Levine, S., Hoenig, E.M., 1968. Induced localization of allergic adrenalitis and encephalomyelitis at sites of thermal injury. J. Immunol. 100 (6), 1310–1318.

Levine, S., Hoenig, E.M., 1971. A new form of localized allergic encephalomyelitis featuring polymorphonuclear neutrophilic leukocytes. Am. J. Pathol. 64 (1), 13–30.

Levine, S., Wenk, E.J., 1967. Rapid passive transfer of allergic encephalomyelitis. J. Immunol. 99 (6), 1277–1285.

Levine, S., Zimmerman, H.M., Wenk, E.J., Gonatas, N.K., 1963. Experimental leukoencephalopathies due to implantation of foreign substances. Am. J. Pathol. 42, 97–117.

Lublin, F.D., Reingold, S.C., Cohen, J.A., Cutter, G.R., Sorensen, P.S., Thompson, A.J., Wolinsky, J.S., Balcer, L.J., Banwell, B., Barkhof, F., Bebo Jr., B., Calabresi, P.A., Clanet, M., Comi, G., Fox, R.J., Freedman, M.S., Goodman, A.D., Inglese, M., Kappos, L., Kieseier, B.C., Lincoln, J.A., Lubetzki, C., Miller, A.E., Montalban, X., O'Connor, P.W., Petkau, J., Pozzilli, C., Rudick, R.A., Sormani, M.P., Stuve, O., Waubant, E., Polman, C.H., 2014. Defining the clinical course of multiple sclerosis: the 2013 revisions. Neurology 83 (3), 278–286.

Lucchinetti, C., Bruck, W., Parisi, J., Scheithauer, B., Rodriguez, M., Lassmann, H., 2000. Heterogeneity of multiple sclerosis lesions: implications for the pathogenesis of demyelination. Ann. Neurol. 47 (6), 707–717.

Maggi, P., Macri, S.M., Gaitan, M.I., Leibovitch, E., Wholer, J.E., Knight, H.L., Ellis, M., Wu, T., Silva, A.C., Massacesi, L., Jacobson, S., Westmoreland, S., Reich, D.S., 2014. The formation of inflammatory demyelinated lesions in cerebral white matter. Ann. Neurol. 76 (4), 594–608.

Mana, P., Fordham, S.A., Staykova, M.A., Correcha, M., Silva, D., Willenborg, D.O., Linares, D., 2009. Demyelination caused by the copper chelator cuprizone halts T cell mediated autoimmune neuroinflammation. J. Neuroimmunol. 210 (1–2), 13–21.

Marik, C., Felts, P.A., Bauer, J., Lassmann, H., Smith, K.J., 2007. Lesion genesis in a subset of patients with multiple sclerosis: a role for innate immunity? Brain 130 (Pt 11), 2800–2815.

Moon, Y., Kim, J.Y., Choi, S.Y., Kim, K., Kim, H., Sun, W., 2011. Induction of ezrin-radixin-moesin molecules after cryogenic traumatic brain injury of the mouse cortex. Neuroreport 22 (6), 304–308.

Narayana, P.A., Doyle, T.J., Lai, D., Wolinsky, J.S., 1998. Serial proton magnetic resonance spectroscopic imaging, contrast-enhanced magnetic resonance imaging, and quantitative lesion volumetry in multiple sclerosis. Ann. Neurol. 43 (1), 56–71.

Nimmerjahn, A., Kirchhoff, F., Helmchen, F., 2005. Resting microglial cells are highly dynamic surveillants of brain parenchyma in vivo. Science 308 (5726), 1314–1318.

Noell, S., Wolburg-Buchholz, K., Mack, A.F., Ritz, R., Tatagiba, M., Beschorner, R., Wolburg, H., Fallier-Becker, P., 2012. Dynamics of expression patterns of AQP4, dystroglycan, agrin and matrix metalloproteinases in human glioblastoma. Cell Tissue Res. 347 (2), 429–441.

Nomachi, A., Yoshinaga, M., Liu, J., Kanchanawong, P., Tohyama, K., Thumkeo, D., Watanabe, T., Narumiya, S., Hirata, T., 2013. Moesin controls clathrin-mediated S1PR1 internalization in T cells. PLoS One 8 (12), e82590.

Oppenheimer, D.R., 1978. The cervical cord in multiple sclerosis. Neuropathol. Appl. Neurobiol. 4 (2), 151–162.

Phillips, M.J., Weller, R.O., Kida, S., Iannotti, F., 1995. Focal brain damage enhances experimental allergic encephalomyelitis in brain and spinal cord. Neuropathol. Appl. Neurobiol. 21 (3), 189–200.

Pines, M., Levi, O., Genin, O., Lavy, A., Angelini, C., Allamand, V., Halevy, O., 2017. Elevated expression of moesin in muscular dystrophies. Am. J. Pathol. 187 (3), 654–664.

Pore, D., Gupta, N., 2015. The ezrin-radixin-moesin family of proteins in the regulation of B-cell immune response. Crit. Rev. Immunol. 35 (1), 15–31.

Prineas, J.W., Parratt, J.D., 2012. Oligodendrocytes and the early multiple sclerosis lesion. Ann. Neurol. 72 (1), 18–31.

Ruther, B.J., Scheld, M., Dreymueller, D., Clarner, T., Kress, E., Brandenburg, L.O., Swartenbroekx, T., Hoornaert, C., Ponsaerts, P., Fallier-Becker, P., Beyer, C., Rohr, S.O., Schmitz, C., Chrzanowski, U., Hochstrasser, T., Nyamoya, S., Kipp, M., 2017. Combination of cuprizone and experimental autoimmune encephalomyelitis to study inflammatory brain lesion formation and progression. Glia 65 (12), 1900–1913.

Scheld, M., Ruther, B.J., Grosse-Veldmann, R., Ohl, K., Tenbrock, K., Dreymuller, D., Fallier-Becker, P., Zendedel, A., Beyer, C., Clarner, T., Kipp, M., 2016. Neurodegeneration triggers peripheral immune cell recruitment into the forebrain. J. Neurosci. 36 (4), 1410–1415.

Schwartz-Albiez, R., Merling, A., Spring, H., Moller, P., Koretz, K., 1995. Differential expression of the microspike-associated protein moesin in human tissues. Eur. J. Cell Biol. 67 (3), 189–198.

Sun, D., Newman, T.A., Perry, V.H., Weller, R.O., 2004. Cytokine-induced enhancement of autoimmune inflammation in the brain and spinal cord: implications for multiple sclerosis. Neuropathol. Appl. Neurobiol. 30 (4), 374–384.

Totaro, R., Di Carmine, C., Splendiani, A., Torlone, S., Patriarca, L., Carrocci, C., Sciamanna, S., Marini, C., Carolei, A., 2016. Occurrence and long-term outcome of tumefactive demyelinating lesions in multiple sclerosis. Neurol. Sci. 37 (7), 1113–1117.

Trepanier, M.O., Hildebrand, K.D., Nyamoya, S.D., Amor, S., Bazinet, R.P., Kipp, M., 2018 Jun. Phosphatidylcholine 36:1 concentration decreases along with demyelination in the cuprizone animal model and in post-mortem multiple sclerosis brain tissue. J. Neurochem. 145 (6), 504–515.

van der Valk, P., De Groot, C.J., 2000. Staging of multiple sclerosis (MS) lesions: pathology of the time frame of MS. Neuropathol. Appl. Neurobiol. 26 (1), 2–10.

van Horssen, J., Singh, S., van der Pol, S., Kipp, M., Lim, J.L., Peferoen, L., Gerritsen, W., Kooi, E.J., Witte, M.E., Geurts, J.J., de Vries, H.E., Peferoen-Baert, R., van den Elsen, P.J., van der Valk, P., Amor, S., 2012. Clusters of activated microglia in normal-appearing white matter show signs of innate immune activation. J. Neuroinflammation 9, 156.

van Noort, J.M., Bsibsi, M., Gerritsen, W.H., van der Valk, P., Bajramovic, J.J., Steinman, L., Amor, S., 2010. Alphab-crystallin is a target for adaptive immune responses and a trigger of innate responses in preactive multiple sclerosis lesions. J. Neuropathol. Exp. Neurol. 69 (7), 694–703.

Vitorino, P., Yeung, S., Crow, A., Bakke, J., Smyczek, T., West, K., McNamara, E., Eastham-Anderson, J., Gould, S., Harris, S.F., Ndubaku, C., Ye, W., 2015. MAP4K4 regulates integrin-FERM binding to control endothelial cell motility. Nature 519 (7544), 425–430.